Version of Record: https://www.sciencedirect.com/science/article/pii/S0040195121004637
Manuscript_f6b6d0bf1f491bc5c685b452c90e2123

Volumetric and shear strain localization throughout triaxial compression experiments on rocks

J. McBeck[1], Y. Ben-Zion[2], and F. Renard[1,3]

[1]Njord Centre, Department of Geosciences, University of Oslo, Oslo, Norway.
[2]Department of Earth Sciences and Southern California Earthquake Center, University of Southern California, Los Angeles, CA, USA.
[3]University Grenoble Alpes, University Savoie Mont Blanc, CNRS, IRD, IFSTTAR, ISTerre, 38000 Grenoble, France.

Corresponding author: J. McBeck, j.a.mcbeck@geo.uio.no

Highlights

- We track strain localization in twelve X-ray tomography triaxial compression experiments.
- The vast majority of the experiments experience strain localization toward brittle failure.
- The maximum strain localization occurs on average at 90% of the failure stress.
- The volumetric (dominantly dilative) strain localizes more than the deviatoric (shear) strain.

Abstract

Deformation localization is a widely observed, but rarely quantified process in the crust. Recent observations suggest that the localization of seismicity and fracture networks can help identify the approach to catastrophic failure. Here, we quantify the localization processes of the volumetric and deviatoric strain components in twelve triaxial compression experiments imaged with X-ray tomography. We capture three-dimensional images of the rock cores during triaxial compressing toward failure, and then calculate the local strain components using digital volume correlation. The divergence and curl of the incremental displacement vector field provide the volumetric and deviatoric components of the strain field. We quantify localization using the proportion of the rock occupied by high magnitudes of the volumetric and deviatoric strains, and the Gini coefficient of these high magnitude strains, which measures the deviation from a uniform process. We find that the vast majority, but not all, of the experiments experience strain localization toward failure. The rocks typically experience their maximum degree of strain localization not immediately preceding failure, but on average at 90% of the failure stress. The volumetric strain tends to localize more than the deviatoric strain. These observations support using the localization of the volumetric strain, along with the deviatoric strain, to identify the evolution of the precursory phase preceding earthquakes.

Key words
Localization; strain; triaxial compression; shear; volumetric; large earthquakes

1. Introduction

Recognizing precursory deformation signals that characterize the preparation phase leading to large failure events is a major goal in geosciences and geotechnical engineering. Recent analysis suggests that increasing localization and clustering of low magnitude seismicity may be a precursory geophysical activity that signals a forthcoming large earthquake (e.g., *Ben-Zion & Zaliapin*, 2020). The long-term localization of deformation and seismicity around and within large crustal fault zones are well-recognized phenomena (e.g., *Powers & Jordan,* 2010; *Tarayoun et al*., 2019; *Mazzotti & Gueydan*, 2018; *Zeng et al*., 2018; *Ben-Zion & Zaliapin*, 2019). Researchers tend to attribute the persistence of seismicity and large-scale displacement along crustal fault zones to the weakness of these zones relative to the surrounding crust. Thus, the evolving strength of the fault zone relative to the crust is a key parameter that controls the localization of deformation.

Crustal faults lose their strength through a long-term evolution from complex fault networks with distributed, isolated segments to more continuous structures (e.g., *Tchalenko*, 1970; *Ben-Zion & Sammis*, 2003). Numerical models and experiments have documented the localization of strain and fault networks from distributed segments to through-going structures (e.g., *Lyakhovsky & Ben-Zion*, 2009; *Autin et al.*, 2013; *Hatem et al.*, 2017). The evolution toward localization around main faults requires that the rate of healing following failure is slower than the rate of the ongoing loading (e.g., *Lyakhovsky et al.*, 2001; *Ben-Zion*, 2008) so the fault zone remains weak relative to the host rock. Rapid healing can prevent localization and lead to the continual generation of broadly distributed failure zones (e.g., *Jamtveit et al.*, 2018). Partial healing of fault zones that remain weaker than the surrounding crust produces cycles of delocalization in interseismic periods, and localization preceding large earthquakes (*Ben-Zion & Zaliapin*, 2020). Here, and throughout the manuscript the term delocalization refers to a decrease in the degree of localization.

On a smaller scale, laboratory observations show an early development of mode-I fractures initially oriented parallel to the maximum compression direction, σ_1, that coalesce under increasing differential stress (*Brace et al.,* 1966; *Tapponnier & Brace*, 1976; *Peng & Johnson*, 1972). Tracking the position of acoustic emissions during triaxial compression reveals the localization of these emissions toward failure, and as the rock supports diminishing axial stress (*Lockner et al.*, 1991). In some experiments, coalescence is such a dominant process in fracture network development that the total number of individual fractures decreases as the total volume of fractures increases (*McBeck et al.*, 2021). Fault and fracture networks may coalesce and evolve to more localized distributions because this reorganization can produce the most mechanically efficient system (e.g., *Cooke & Madden*, 2014; *McBeck et al.*, 2017; *Hatem et al.*, 2017). More continuous faults may concentrate deformation on faults (slip) and reduce the magnitude of internal deformation of the host rock to a greater extent than systems with many isolated, smaller faults. Thus, a more localized fault network may also be the more efficient fault network.

The observations of localization in 1) nominally intact rocks from isolated mode-I fractures to linked, through-going faults, 2) crustal fault networks from isolated to continuous structures, and 3) seismicity preceding large earthquakes, suggest that tracking localization of deformation may help indicate the timing of catastrophic failure. Indeed, machine learning analyses suggest that statistics that describe the spatial distribution of localizing fracture networks are critical for successfully predicting the timing of macroscopic failure in triaxial compression experiments (*McBeck, Aiken, Mathiesen et al.,* 2020). Similarly, machine learning analyses indicate that the spatial distribution of the fracture network controls whether individual fractures grow (*McBeck et al.*, 2019). Thus, the spatial distribution of the fracture network controls both local failure (individual fracture growth) and global failure (system-size, catastrophic failure).

Additional experimental observations that can reveal localization during rock deformation, and help predict the timing of failure, include the local strain fields captured during triaxial compression experiments imaged with X-ray tomography. In these experiments, researchers acquire three-dimensional images of rock cores during triaxial compression. The images enable calculating the evolving local strain tensor throughout the rocks using digital volume correlation analysis (e.g., *Charalampidou et al.*, 2011; *Ji et al.*, 2015; *McBeck et al.*, 2018; *Shahin et al.*, 2019; *Stamati et al.,* 2019; *Heap et al.*, 2020; *Mao et al.*, 2021; *Baud et al.*, 2021). Using such time series of strain fields, machine learning analyses indicate that the intermediate values of the dilative strain can predict the timing of system-scale failure in these experiments (*McBeck, Aiken, Ben-Zion et al.,* 2020). Thus, the magnitude of the dilative strain helps signal imminent system-scale failure in these experiments.

In the present study, we analyze the evolving strain localization to constrain the reliability of this process when identifying the proximity of catastrophic failure. If the localization of the strain field is not relatively systematic toward failure, then this process may be a poor predictor of the proximity of failure. We quantify strain localization in twelve triaxial compression experiments imaged with X-ray tomography, including experiments on Fountainebleau sandstone, Mount Etna basalt, monzonite, Westerly granite, Green River shale, and Andstrude limestone (**Table** 1). We track localization using the proportion of the rock volume that is occupied by relatively high magnitudes of the strain components, including the volumetric (dilative) and deviatoric (shear) strain, and the Gini coefficient derived from the Receiver Operating Characteristic framework (e.g., *Ben-Zion & Zaliapin*, 2020). When the proportion of the rock volume occupied by high strain values decreases, or the Gini coefficient increases, the rock experiences higher degree of strain localization. We compare the maximum observed localization (i.e., minimum proportion of volume occupied by high magnitude strains and maximum Gini coefficient) of both strain components throughout twelve experiments.

In a previous analysis using the same set of experiments analyzed here, we examined how four strain components, the contraction, dilation, left-lateral shear strain, and right-lateral shear strain, interacted with each other (*McBeck, Ben-Zion et al.*, 2020). To quantify the localization of the complete strain population of each component, this previous work calculated the volume of rock occupied by each of the strain components, including both lower and higher magnitude strains. In the experiments, the dilative strain occupies larger volumes with increasing differential stress, while the contractive strain occupies smaller volumes. In contrast, the left- and right-lateral shear strains do not tend to occupy larger and larger volumes. This result occurs because of the competition between dilation and contraction, and the dominance of dilation under higher differential stress. In contrast, the left-lateral shear strain does not consistently dominate the right-lateral shear strain, or vice versa.

The analysis of the present work is motivated by the observations of localizing seismicity before major earthquakes in southern and Baja California (e.g., *Ben-Zion & Zaliapin*, 2020). Following these field results, we examine the localization of the largest magnitudes of the strain components, rather than the complete strain populations. Moreover, we compare the localization of the volumetric component, including both the dilation and contraction, to that associated with the deviatoric component. This analysis thus benefits from the fact that comparing the localization properties of the volumetric and deviatoric components of the strain field is not obscured by the increasing volume fraction of dilation.

The results of the present work indicate that the volumetric strain, as measured with the absolute value of the divergence of the incremental displacement vector field calculated from DVC, localizes more than the deviatoric strain, as measured with the absolute value of the curl of the incremental displacement vector field. We compare the timing of when each experiment achieves its maximum localization. We find that the vast majority of the experiments experience maximum localization beyond 75% of the failure stress, however, less than half of the experiments experience their maximum localization immediately preceding failure. In contrast to the idea that increasing localization will drive more localization, the rocks do not experience a continual increase in localization throughout the experiments. We compare the change in the magnitude of localization throughout each experiment using the difference between the maximum and minimum localization in each experiment, along with the difference between the localization observed in the strain fields immediately preceding failure and at the onset of loading. The results show that >80% of the experiments host strain fields that increase in localization toward failure. Consistent with the greater magnitudes of localization of the volumetric strain, the volumetric strain also experiences the greatest increases in localization from the onset of loading to failure, and from the maximum to minimum observed localization. This analysis thus reveals two key findings: 1) rocks do not tend to experience their maximum strain localization immediately preceding failure, but on average near 90% of the failure stress, and 2) the volumetric strain tends to localize more than deviatoric strain in terms of both the absolute minimum and the change in localization.

2. Methods

2.1. Experimental conditions

Previous studies describe the conditions of the analyzed experiments (e.g., *Renard et al.*, 2017, 2018; *Renard, McBeck, Cordonnier et al.*, 2019; *Renard, McBeck, Kandula et al.*, 2019; *McBeck et al.*, 2019; *McBeck et al.*, 2018), so we only summarize the pertinent details here. We deform two cores of six types of rocks, including Fontainebleau sandstone, Mount Etna basalt, monzonite, Westerly granite, Green River shale and Anstrude limestone (**Table** 1). The rock cores are 1 cm tall and 4-5 mm wide cylinders (**Table** 1). We core the shale parallel to bedding.

We triaxially compress the rock cores on beamline ID19 at the European Synchrotron and Radiation Facility inside the Hades apparatus (*Renard et al.*, 2016), while acquiring tomograms. The tomograms provide three-dimensional fields of linear attenuation coefficients, indicative of X-ray energy and local density. We apply confining stresses of 5-35 MPa (**Table** 1) and increase the axial stress in steps of 0.5-5 MPa until the sample fails in a sudden stress drop. After each stress step, we acquire a tomogram within two minutes. The high quality of the tomograms, including the lack of significant blurring, indicates that the rocks do not deform during scan acquisition.

rock type	**experiment number**	**confining stress (MPa)**	**sample diameter (mm)**	**# of X-ray tomograms**
Fontainebleau sandstone	#1	20	5	184
	#2	10	5	47
Mount Etna basalt	#1	10	4	32
	#2	10	4	36
monzonite	#4	35	4	65
	#5	25	4	80
Westerly granite	#2	5	4	30
	#4	10	4	66
Green River shale	#2	20	5	60
	#3	20	5	61
Anstrude limestone	#2	20	5	41
	#5	5	5	26

Table 1. Rock types, applied confining stress, diameter of rock cylinders, and numbers of X-ray tomograms acquired in twelve rock deformation experiments.

2.2. Digital volume correlation analysis

We use the code TomoWarp2 (*Tudisco et al.*, 2017) to perform the digital volume correlation analysis. This analysis searches for similar patterns of voxels in pairs of tomograms, or other three-dimensional images, and then calculates the displacement vector that best maps one set of voxels to the other (e.g., *Charalampidou et al.*, 2011; *Ji et al.*, 2015; *McBeck et al.*, 2018; *Shahin et al.*, 2019; *Stamati et al.,* 2019; *Heap et al.*, 2020; *Mao et al.*, 2021; *Baud et al.*, 2021). In TomoWarp2, the node spacing determines the spatial resolution and the correlation window size determines the size of the volume used to identify similar patterns of voxels. Using a node spacing of 20 voxels (0.13 mm) and correlation window size of 10 voxels (65 µm) produces a good spatial resolution and reasonable levels of signal to noise. *McBeck et al.* (2018) describe the influence of varying these parameters on the calculated displacement fields.

Following the approach of our previous analyses (e.g., *McBeck et al.*, 2018), we subdivide each experiment into approximately eight to ten equal increments of macroscopic axial contraction, and then perform DVC on the resulting pairs of tomograms. Thus, we calculate the incremental displacement field between each tomogram pair. To compare the varying evolution of the volumetric and deviatoric components of the strain field, we calculate the divergence (volumetric, contractive and dilative) and curl (deviatoric, shear) of the displacement fields. The divergence fields thus include both contractive and dilative strains. With increasing differential stress, a larger volume of the rock experiences dilation and a smaller volume experiences contraction in these experiments (*McBeck, Ben-Zion et al.*, 2020). The deviatoric component of the strain tensor may be represented with different metrics, such as the Von Mises strain. We follow the approach of the geodetic community (e.g., *Bennett et al.*, 2003; *Bos et al.*, 2003) by decomposing the strain tensor into its volumetric and deviatoric components using the divergence and the curl. The curl indicates the rotation of a field, and thus captures the influence of the six shear strain components of the three-dimensional strain tensor. In two-dimensions, the curl is equal to the shear strain.

To ensure that the magnitude of macroscopic strain done between scan acquisitions does not strongly influence the calculated incremental strains, we divide the incremental divergence and curl values by the macroscopic axial contraction done during the given scan acquisition. Thus, the DVC analysis provides a time series of the incremental normalized divergence and curl fields throughout the rock at eight to ten unique time steps in each experiment with a spatial resolution of 0.13 mm.

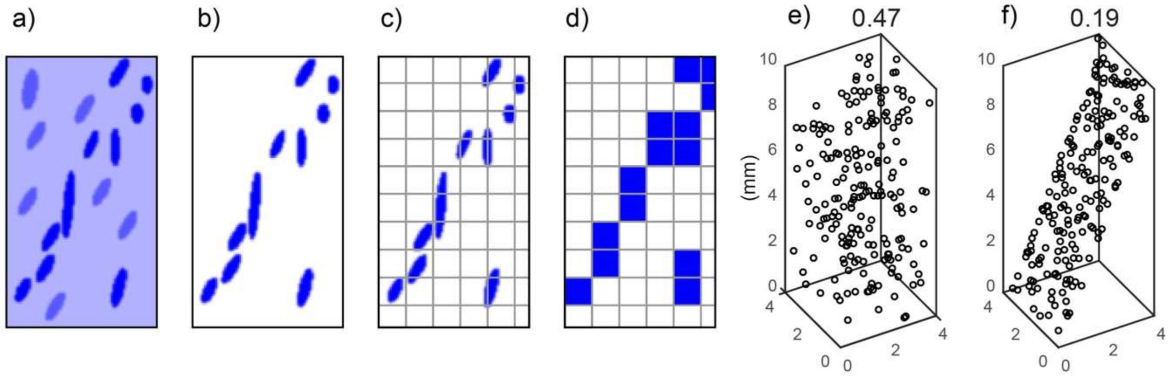

Figure 1. An illustration of the method of calculating the proportion of volume occupied by high magnitudes of strain. The DVC analysis provides a discretized field of continuous strain values at a spatial resolution of 0.13 mm (a). To quantify spatial localization, we first extract the high magnitudes of strain, using a range of percentile thresholds (b). Then, we subdivide the strain field into cubes with side lengths of 0.25 mm, 0.5 mm, or 1 mm (c). Finally, we identify the cubes that host high magnitudes of strain (d). We then calculate the proportion of the rock occupied by the high strain values using the grid of cubes, i.e., the volume of blue cubes divided by the total volume. In this synthetic example with a grid spacing of 1 mm (e-f), the more distributed strain field produces a volume proportion of 0.47, while the more localized strain field produces a volume proportion of 0.19. Thus, when the high strain magnitudes are spread diffusely throughout the system (e), the resulting volume proportion is higher than when the high strains are localized along a plane (f).

2.3. Quantifying localization

To quantify localization using the time series of incremental divergence and curl fields, we follow the approach of *Ben-Zion & Zaliapin* (2020). We track the volume of rock occupied by high magnitudes of local strain, and we calculate the Gini coefficient. The Gini coefficient measures the inequality in a population, and thus can indicate the dispersion or localization of a population (e.g., *Gini*, 1921). We measure the Gini coefficient as twice the area between the Receiver Operating Characteristic curve and the diagonal line that is indicative of a uniform distribution (**Figure** S1).

Whereas *Ben-Zion & Zaliapin* (2020) calculated the fractional area of a grid of 2D cells occupied by seismicity in southern and Baja California, we identify the fractional volume of a grid of cubes occupied by high magnitudes of (incremental) divergence and curl at each time step of each experiment (**Figure** 1). This approach requires selecting two parameters: the size of the cubes and the threshold used to select the high magnitudes of the strain. We vary the size of the cubes from 0.25-1 mm, and the threshold from 70-90th percentile. We tested thresholds of these larger percentiles because the largest local strains have the strongest influence on the global strain field, and thus on the localization properties. We tested cube sizes with a minimum length scale of 0.25 mm because this value is twice the spatial resolution of the DVC analysis. If we use a cube size equal to the spatial resolution of the DVC analysis, the volume of rock occupied by strain values above a given percentile would remain constant throughout the experiment. We show that varying these parameters does not influence the central conclusions of the analysis (**Section** 3.3, **Figure** S2). To quantify localization, we 1) extract the absolute value (magnitude) of the incremental divergence and curl fields that are above a given percentile threshold in a particular time step, 2) count the number of cubes that these high strains occupy, and 3) divide this number by the total number of cubes in the rock (**Figure** 1). We then report this proportion as a percentage. We also show that using the Gini coefficient to quantify localization produces the same central results as the analysis performed using the proportion of volume occupied by high magnitudes of strain (**Figure** S2).

Thus, we use the incremental strain done between scan acquisitions to quantify the spatial localization of the strain field. This process is analogous to the method by which seismologists track the localization of seismicity (e.g., *Ben-Zion & Zaliapin*, 2020). In both analyses, we extract the incremental deformation (strain or seismicity) done within a certain time interval. Thus, following this approach, we describe decreases in the spatial localization of the incremental deformation as delocalization, and identify the time when the high incremental strains are the most localized as the timing of maximum localization.

3. Results

3.1. Qualitative observations of strain localization

In the time series of strain fields captured during triaxial compression, we observe qualitatively that the high magnitudes of incremental strains appear to localize with increasing differential stress. Under low differential stress, the high magnitudes (>90th percentile) of the strain fields appear diffusely distributed throughout the rock core (**Figure** 2). Under higher differential stress, they appear to localize or cluster. Based on visual inspection and qualitative comparison, some of the strain fields appear more localized than others. For example, the strain fields observed in the granite experiment immediately preceding failure (stress step #8 in **Figure** 2b) appear more localized than those observed in the sandstone experiment immediately preceding failure (stress step #10 in **Figure** 2a). In addition, the degree of localization of the volumetric and deviatoric strain fields appear to differ at a given time in a particular experiment. For example, the volumetric strain field in the granite experiment immediately preceding failure appears more localized than the deviatoric strain field at this time step. In the subsequent sections, we test these qualitative observations by quantifying the localization of the high magnitudes of the volumetric and deviatoric strains.

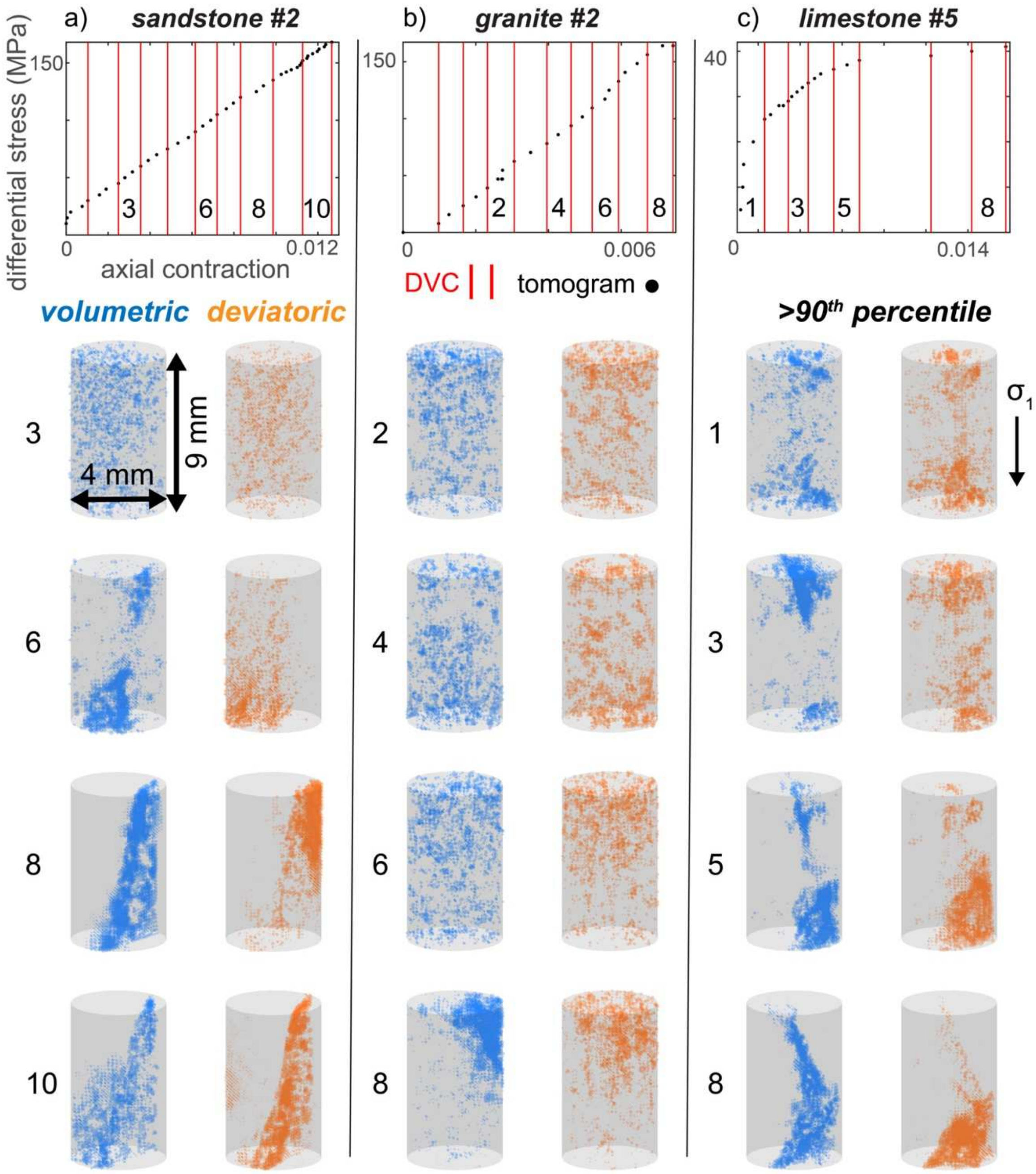

Figure 2. Example snapshots of local incremental strain fields in three experiments: a) sandstone #2, b) granite #2, and c) limestone #5**.** The first row shows the differential stress-axial strain evolutions for each experiment, including the conditions when we acquired a tomogram (black dots) and the tomogram pairs we used in the DVC analysis (red lines). The numbers in the plots correspond to the numbered cores shown below. The cores show the location of the absolute values of the volumetric (blue) and deviatoric (orange) local incremental strain values that are above the 90th percentile of the population of these respective strain components.

3.2. General evolution of localization toward failure

Tracking the proportion of the rock volume occupied by high magnitudes of strain suggest that the strain fields localize with increasing differential stress (**Figure** 3), consistent with our qualitative observations (**Figure** 2). Here, we focus on the results derived from extracting the strain values above the 90th percentile, and calculating the proportion of the volume occupied by high magnitudes of strain in a grid with a spacing of 0.5 mm. In a subsequent section, we show that the chosen threshold and grid spacing do not significantly influence the central results.

The general trends of these evolutions show that the local incremental high strain values tend to occupy less space (i.e., localize) as the rocks approach failure (**Figure** 3). Here, we focus on three example experiments that show the range in localization behavior observed in all of the experiments. In some experiments, the strain fields systematically localize toward failure, such as the granite #2 experiment (**Figure** 3b). In other experiments, such as the sandstone #2 and limestone #5 experiments, the strain fields localize and then delocalize toward failure: decreasing and then increasing in the proportion of occupied volume. Thus, the maximum localization of the strain field (minimum proportion occupied) does not occur immediately preceding failure in the sandstone #2 and limestone #5 experiments, but does occur at this critical time in the granite #2 experiment.

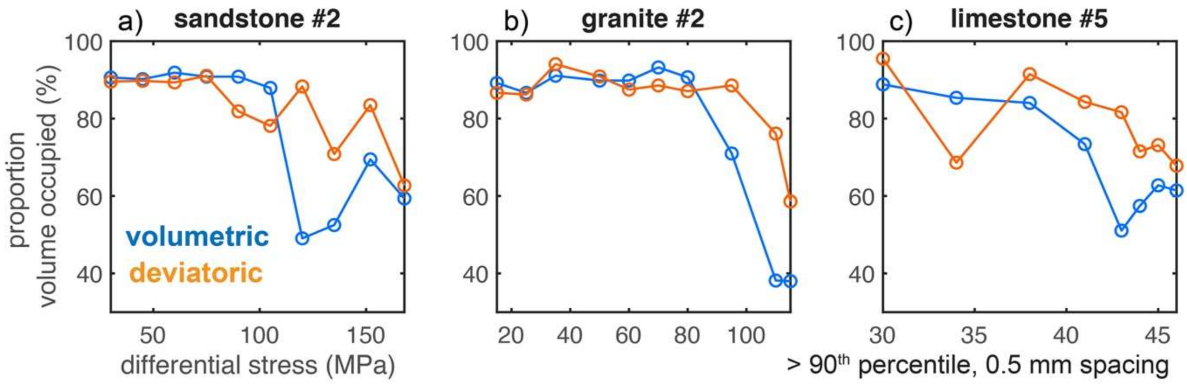

Figure 3. Evolutions of strain localization in three example experiments: a) sandstone #2, b) granite #2, and c) limestone #5. The blue and orange lines show the proportion of the volume occupied by high magnitudes (>90th percentile) of the volumetric and deviatoric strain, respectively, using a grid with 0.5 mm spacing.

This quantification of the localization (**Figure** 3) enables directly comparing the magnitude of strain localization in the volumetric and deviatoric strain components. In all three experiments, the high magnitudes of the deviatoric strain occupy more volume than the high magnitudes of the volumetric strain immediately preceding failure. The difference between the proportion occupied by the volumetric and deviatoric strain immediately preceding failure is the largest in the granite #2 experiment, 20%, and smallest in the sandstone #2 experiment, 2%. Thus, the volumetric strain is more localized immediately preceding failure than the deviatoric strains in these experiments. In the subsequent sections, we compare these results in all twelve experiments, including the timing and magnitude of the maximum localization of the volumetric and deviatoric strains.

3.3. Maximum localization during triaxial compression

The example evolutions (**Figure** 3) highlight two key aspects of strain localization on which we now focus in greater depth as we analyze the twelve experiments. First, we identify the minimum proportion of the rock volume occupied by the high magnitudes of strain throughout all the experiments, for both the volumetric and deviatoric strain components (**Figure** 4). Then, we compare the magnitude of the greatest localization achieved by the volumetric and deviatoric strains, and examine the timing of when the rocks experienced this maximum localization.

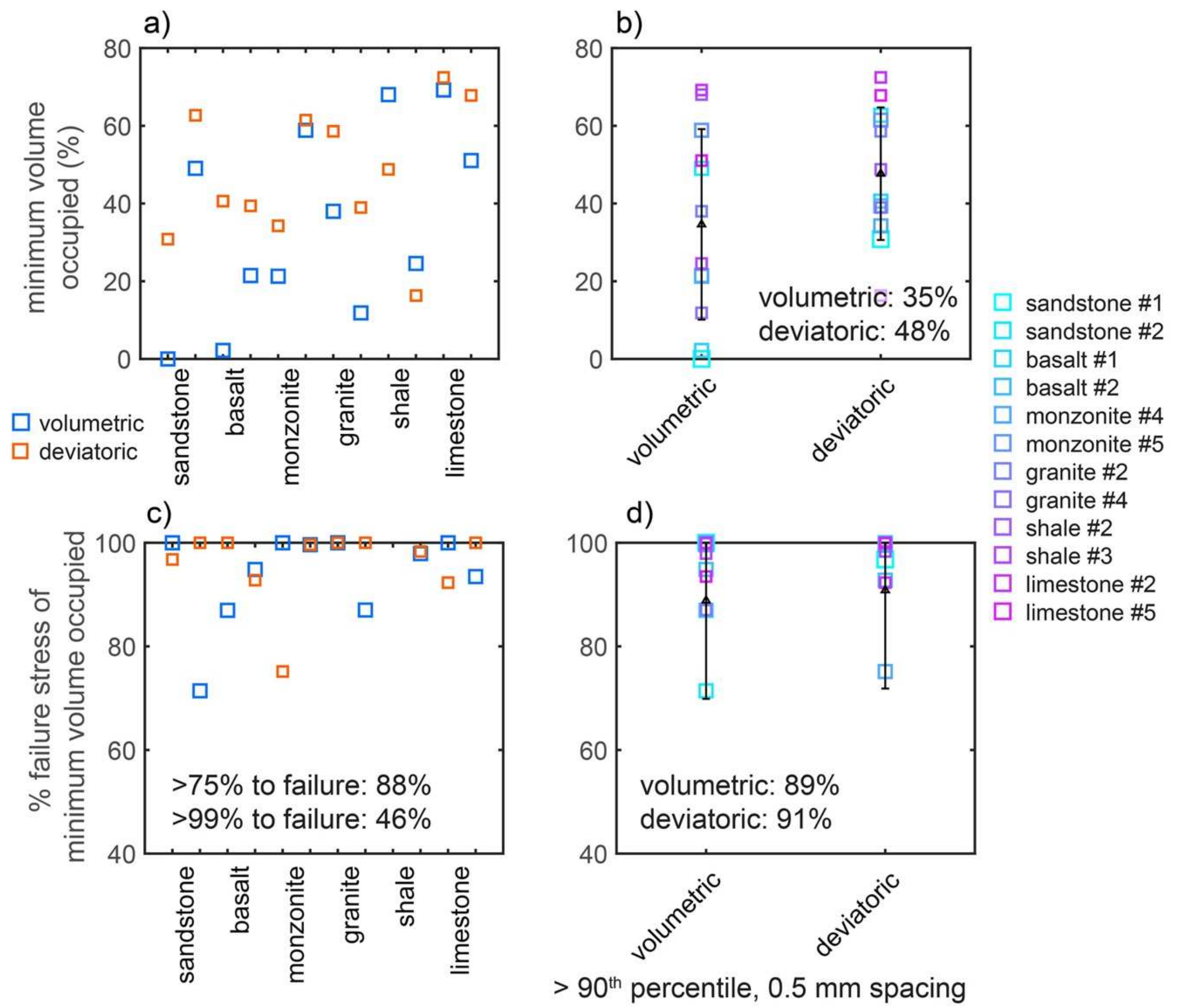

Figure 4. Minimum volume occupied by high magnitude strains in all experiments (a-b), and timing of the maximum localization (c-d). a, c) Data organized by experiment. Each rock type label corresponds to data from two experiments. b, d) Data organized by strain component. c-d) The timing of maximum localization is shown by the percent of the differential stress at failure of the strain field, i.e., 100% is at failure. b) The black symbols show the mean ± one standard deviation of the minimum proportion achieved for each strain component across all the experiments. The numbers in the lower right corner list the means of the minimum proportion: 35% for the volumetric strain and 48% for the deviatoric strain. c) The percentages at the bottom of the plot show the proportion of the measurements (two strain components for each of the twelve experiments) that achieve their maximum localization >75% of the failure stress (88%) and >99% of the failure stress (46%). d) The black symbols show the mean ± one standard deviation of the timing of maximum localization for each strain component. The numbers in the lower left corner list the means of this timing: 89% for the volumetric and 91% for the deviatoric.

Figure 4a shows the minimum proportion of rock volume occupied throughout each experiment, and thus the maximum localization achieved by each experiment. The results indicate that the rock type does not exert a clear influence on the maximum localization achieved in each experiment. For example, the two sandstone experiments are among the experiments that experience the weakest and strongest localization, from about 60% of the minimum proportion occupied to near 0%. Similarly, the two shale experiments exhibit a wide range of the maximum achieved localization.

Figure 4b compares the minimum proportion of rock volume occupied by the high magnitudes of the volumetric strain to the high magnitudes of the deviatoric strain. This comparison indicates that the volumetric strain achieves lower proportions than the deviatoric strain, and thus greater localization. The average of the minimum proportion occupied across all of the experiments is 35% for the volumetric strain, and 48% for the deviatoric strain (**Figure** 4b). In addition, ten of the twelve experiments host volumetric strain fields that localize more than the deviatoric strain: only the two shale experiments show the opposite trend. Thus, the volumetric strain tends to achieve greater localization throughout the experiments than the deviatoric strain.

Next, we examine the timing of when the rocks experience their maximum localization (**Figure** 4c-d). We use the differential stress exerted on the rock as a proxy for time, and report the percent of the failure stress of the differential stress at the time when we acquired the second tomogram used in the DVC calculation that hosts the maximum localization. We find that 88% of the experiments achieve their maximum localization at >75% of the failure stress (**Figure** 4c). However, only 46% of the experiments achieve their maximum localization at >99% of the failure stress, immediately preceding failure. Thus, the vast majority of the experiments experience their maximum localization in the final stages of the experiment, but less than half of the experiments experience their maximum localization immediately preceding failure. Comparing the difference between the timing of maximum localization of the volumetric and deviatoric strains indicates that the rocks experience the maximum localization of the volumetric strain at similar times as the deviatoric strain (**Figure** 4d). The mean of the timing of maximum localization of the volumetric and deviatoric strain across all of the experiments only differ by 2%, from 89-91%. Thus, both strain components experience their maximum localization not immediately preceding failure, but within about 10% of the failure stress on average.

3.4. Change in localization throughout triaxial compression

Next, we examine how the magnitude of localization changes throughout each experiment (**Figure** 5). We track this change with the difference between the minimum and maximum proportion of the rock volume occupied throughout the full experiment, and the difference between the proportion of the rock volume occupied in the final (preceding failure) and initial (at the onset of loading) strain fields.

Using the difference between the proportion of volume occupied by high magnitude strains at the final and initial stage, most of the experiments experience localization. In particular, 83% of the measurements of the combination of experiments and strain components, have a negative difference in the proportion occupied between the final and initial stages, indicating that the proportion was smaller at the end of the experiment than at the beginning (**Figure** 5c). The exceptions to this trend, in which the strain field delocalizes from the onset of loading to immediately preceding failure, include both strain components in the shale #2 experiment, the volumetric strain in the shale #3 experiment, and the deviatoric strain in the limestone #2 experiment. Thus, the rock types that experience delocalization tend to be those that experience more ductile or plastic processes: the shale and limestone. Similarly, the rock types that experience the greatest increases in localization tend to be those that are dominated by brittle processes: sandstone and basalt.

Both of the metrics of the change in localization indicate that the volumetric strains tend to localize more than the deviatoric strains. In particular, the mean of the difference between the minimum and maximum proportion occupied across all experiments is -54% for the volumetric strain and -40% for the deviatoric strain (**Figure** 5b). In addition, all of the experiments except the shale #2 experiment show greater increases in localization for the volumetric strain than the deviatoric strain. Similarly, the mean of the change in the proportion occupied from the initial to the final stage across all the experiments is -36% for the volumetric strain and -29% for the deviatoric strain. Of the experiments in which both strain components localize, all but one (limestone #5) show greater localization from the initial to final stage of the volumetric strain than the deviatoric strain. The exceptional limestone #5 experiment shows about equal degrees of localization in the strain components. Thus, the increase in the localization of the volumetric strain generally tends to exceed the increase of the deviatoric strain.

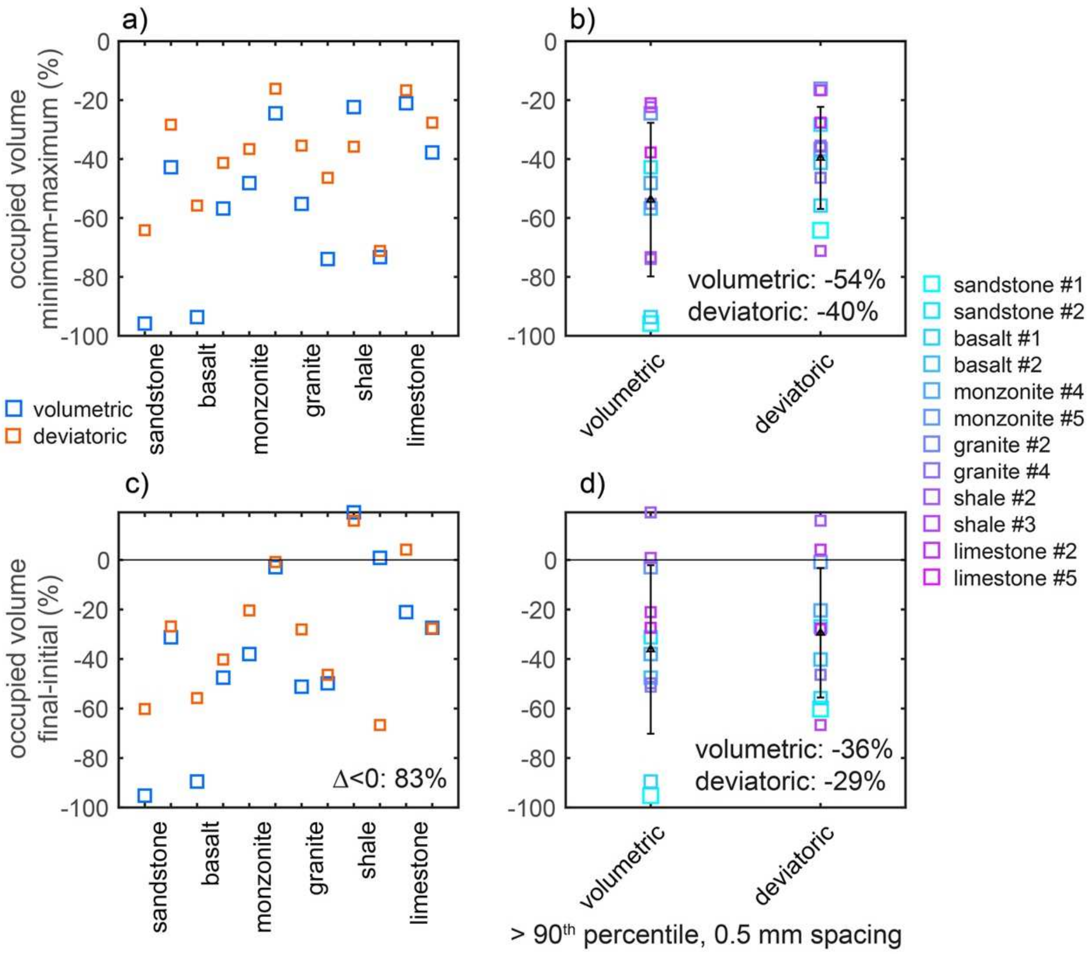

Figure 5. Difference in localization through time: a-b) difference between the minimum and maximum proportion of the rock volume occupied, c-d) difference between the proportion of the rock volume occupied in the final (preceding failure) and initial (at the onset of loading) strain fields. a, c) Data organized by experiment. Each rock type label corresponds to data from two experiments. b, d) Data organized by strain component. b, d) The black symbols show the mean ± one standard deviation of the difference in the proportion occupied for the volumetric and deviatoric strain components, and the text lists the means. b) The mean of the greatest decrease in the proportion of volume occupied across all the experiments is -54% for the volumetric strain and -40% for the deviatoric strain. d) The mean of the change in the proportion occupied from the initial to the final stage across all the experiments is -36% for the volumetric strain and -29% for the deviatoric strain. c) The percentage in the bottom right corner shows the percentage of measurements in which the change in the proportion of the volume occupied is negative, and thus the experiments that experience localization.

3.5. Sensitivity of the results to the parameters

The results depend to some extent on the chosen threshold to select the high magnitudes of strain, and the spacing of the grid used to calculate the proportion of the occupied volume. First, we examine how the results change as we change the threshold, and keep the grid spacing constant (**Figure** 6). Increasing the threshold from the 70^{th} to 90^{th} percentile reduces the mean minimum proportion of rock occupied by the high strain component (**Figure** 6a). This trend is expected as higher percentile thresholds lead to lower numbers of high magnitude strains. For each threshold, the volumetric strain achieves lower minimum occupied proportions than the deviatoric strain. Thus, this central conclusion remains consistent with these varying thresholds.

Changing the threshold does not strongly influence the identified timing of the maximum localization (**Figure** 6b), producing similar timings for the volumetric and deviatoric strain. Increasing the threshold increases the negative difference between the proportion occupied in the final and initial stages, and difference between the minimum and maximum localization (**Figure** 6c-d). This trend is expected as higher percentile thresholds lead to lower numbers of high strain magnitudes. For both metrics of the change in localization, the volumetric strain localizes more than the deviatoric strain for all of the examined thresholds. Thus, this central conclusion again remains consistent with these varying thresholds.

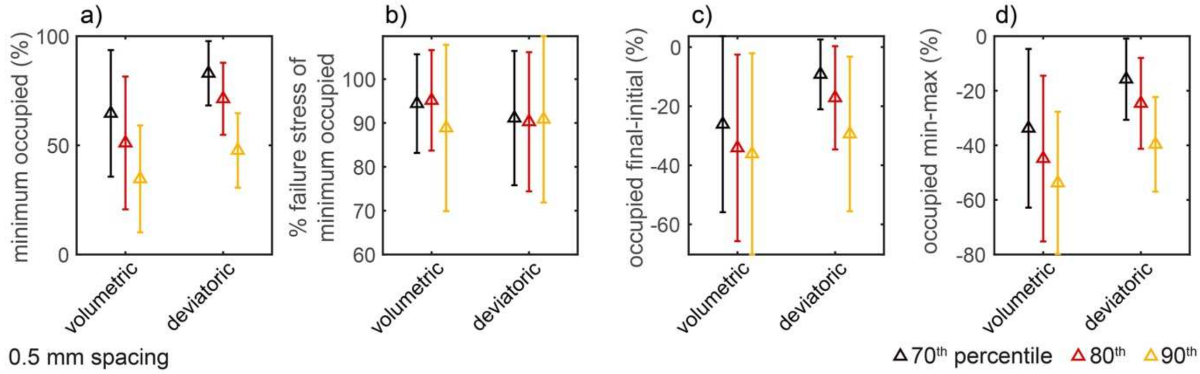

Figure 6. The influence of percentile threshold used to identify the high strain values with constant grid spacing (0.5 mm) on a) the minimum proportion occupied, b) the timing when the minimum proportion is occupied, c) the difference between the proportion of the final and initial stage, and d) the difference between the minimum and maximum proportion occupied. Each value is the mean ± one standard deviation of the measurement across all the experiments.

Next, we examine the influence of the grid spacing with a constant threshold (**Figure** 7). Increasing the grid spacing from 0.25 mm to 1 mm (e.g., **Figure** 1) increases the minimum proportion of rock volume occupied (**Figure** 7a). This trend is expected because larger grid sizes provide greater opportunity for high magnitudes of strain to fall within a particular cube. Thus, larger grid sizes are expected to produce lower resolution results, and an apparent delocalizing effect on the calculated minimum proportion of rock volume occupied by high magnitudes of strain. Nevertheless, for each examined grid spacing, the minimum proportion of the rock occupied by high magnitudes of volumetric strain is lower than the proportion occupied by the deviatoric strain. This trend supports the central observation that the volumetric strain localizes more than the deviatoric strain.

Increasing the grid spacing does not systematically influence the identified timing of the maximum localization (**Figure** 7b), producing similar timings of the volumetric and deviatoric strain. Increasing the grid spacing tends to decrease the (negative) difference between the proportion occupied in the final and initial stages, and difference between the minimum and maximum localization (**Figure** 7c-d). This trend is expected from the lower resolution, larger grid sizes. For both metrics of the change in localization, the volumetric strain localizes more than the deviatoric strain for all the examined grid sizes, supporting this central conclusion.

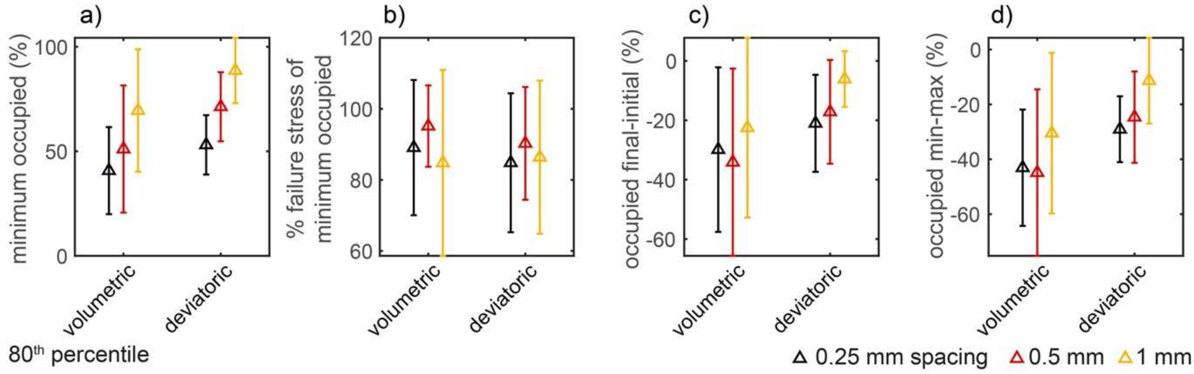

Figure 7. The influence of grid spacing with constant threshold (80th percentile) on a) the minimum proportion occupied, b) the timing when the minimum proportion is occupied, c) the difference between the proportion of the final and initial stage, and d) the difference between the minimum and maximum proportion occupied. Each value is the mean ± one standard deviation of the measurement across all the experiments.

In order to test the robustness of these conclusions, we also track localization using the Gini coefficient. This coefficient measures the inequality in a distribution of values (e.g., *Gini*, 1921). The central results of the analysis shown in depth here do not vary when we use the Gini coefficient to track localization (**Figure** S2). In particular, using the Gini coefficient of the high magnitudes of strain and the proportion of the rock volume occupied by this strain, we observe that 1) the volumetric strain localizes more than the deviatoric strain, 2) the majority of the experiments localize from the onset of loading to immediately preceding failure, and 3) the experiments achieve their maximum localization not at failure, but on average near 90% of the failure stress.

4. Discussion

4.1. Timing of maximum localization

In twelve triaxial compression experiments imaged with X-ray tomography, we observe that the local incremental strain fields tend to localize from the onset of loading to immediately preceding failure in qualitative representations of the data (**Figure** 2), and in our localization statistics (**Figure** 3, **Figure** S2). Using a 90th percentile threshold to select the high magnitudes of strain, and 0.5 mm grid spacing to calculate the proportion of the rock volume occupied by these high magnitudes, 83% of the strain components measured in each experiment show localization from the initial to final stage of the experiment (**Figure** 5).

If strain localization follows a systematic evolution, steadily increasing toward system-scale failure, we would expect the highest degree of localization just before failure. To test this idea, we identified the differential stress at which the rocks achieve the largest degree of strain localization (**Figure** 4). We observe that contrary to this expectation, some rocks do not achieve their maximum strain localization immediately preceding failure, but on average near 90% of the failure stress. For the majority of experiments (>50%), the rocks experience episodes of localization and delocalization that cause the maximum strain localization to occur near 90% of the failure stress (**Figure** 5). Thus, the strain fields tend to localize with the greatest magnitude following yielding, but before the final system-size failure (e.g., **Figure** 8b). After 90% of the failure stress on average, the strain field delocalizes to some extent before the rock macroscopically fails.

These results agree with observations of localizing seismicity prior to *M*>7 earthquakes in southern and Baja California between 1983-2019. *Ben-Zion & Zaliapin* (2020) tracked the proportion of the area occupied by low magnitude seismicity prior to the 1992 Landers, 1999 Hector Mine, 2010 El Mayor-Cucapah and 2019 Ridgecrest earthquakes. They observed that the proportion of area occupied by low magnitude seismicity decreased prior to all four large earthquakes (*Ben-Zion & Zaliapin*, 2020; Figures 7 and 9). For the Landers, Hector Mine and El Mayor-Cucapah earthquakes, the low magnitude seismicity occupied the smallest fractional area 2-3 years before the large events, and then delocalized in the last few months before the mainshocks. For the Ridgecrest earthquake, the observed localization process continued until the time of the large earthquake. These trends partially depend on the parameters used in the analysis (*Ben-Zion & Zaliapin*, 2020). However, varying the parameters does not change the observation that the maximum localization occurs earlier than immediately before most of the examined *M*>7 earthquakes. The evolution of localization and subsequent delocalization just prior to large failure for some earthquakes is consistent with our experimental observations: while 88% of the experiments achieve their maximum localization at >75% of the failure stress, only 46% of the experiments experience their maximum localization at >99% of the failure stress. The delocalization immediately preceding some large earthquakes and system-size failure in the laboratory experiments may arise because of the stress transfer produced by progressively larger events approaching catastrophic failure. As larger and larger events develop, their perturbation of the stress field may bring larger and larger volumes of rock closer to failure, and thus promote failure away from largest structures, i.e., delocalization (e.g., **Figure** 8b).

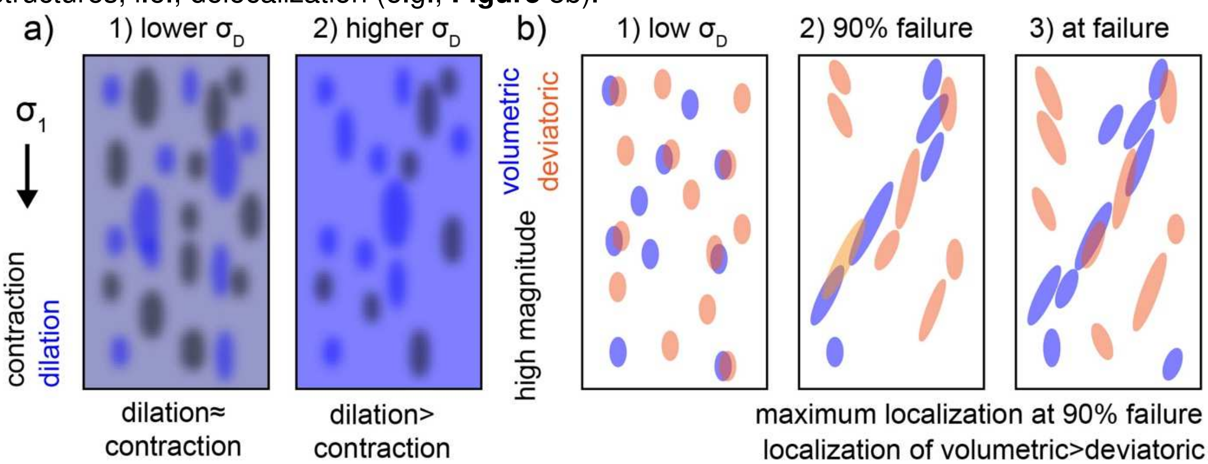

Figure 8. Summary of observations of a) strain accumulation from previous analyses on the experiments analyzed here (*McBeck, Ben-Zion, et al.*, 2020), and b) strain localization from the present analysis. a) Competition between dilation and contraction. Under lower differential stress, the volume of rock that undergoes dilation is similar to the volume that undergoes contraction. Under higher differential stress, the rock experiences a higher volume fracture of dilation than contraction. In contrast to the evolution of the volumetric strains, the shear strain components do not evolve to favor one sense of shear rather than the other. Instead, the rock experiences similar volumes of left-lateral and right-lateral shear strain throughout loading. b) Localization behavior of high magnitude strains observed in experiments. The volumetric and deviatoric strains localize toward failure in the majority of the experiments. The maximum localization occurs near 90% of the failure stress (#2), rather than immediately preceding failure (#3). The volumetric strain localizes more than the deviatoric strain.

Additional geophysical observations that span the 20th century similarly support the idea that localization of seismicity precedes large earthquakes. *Zeng et al.* (2018) tracked the spatial distribution of *M*≥4 seismicity throughout California and Nevada. From 1933-1980, the seismicity was broadly distributed, and few high magnitude earthquakes occurred in this region. Following the 1980s, seismicity began to localize around the main fault systems, and several *M*>7 earthquakes occurred. *Zeng et al.* (2018) attribute these cycles of delocalization and localization to the stress reduction that occurs after large earthquakes and the resulting stress shadow. They postulate that the 1906 *M*7.8 San Francisco earthquake and 1857 *M*7.9 Fort Tejon earthquake reduced stresses in the region. These stress reductions allowed the seismicity to remain diffusely distributed for several decades. Then, as tectonic loading reduced the stress shadow, the main fault system entered a new phase of localization in the late 1980s that led to larger earthquakes.

Following yielding and near 90% of the failure stress in our experiments, fracture growth and coalescence and subsequent opening and slip along these fractures, may provide temporary stress shadows within the rock core. Deformation within the rock may relieve the accumulated stresses prior to the final macroscopic failure event to a sufficient extent to promote delocalization. The stress transfers from the large failures in the localizing zone could induce failure outside the localization zone, thereby triggering delocalization. The competition between weakening in failing zones leading to localization, and factors that produce partial delocalization, may explain why about half of the experiments show delocalization just prior to failure, while the other experiments show maximum localization immediately preceding failure. In particular, the loading rate, fracture propagation rate, and coalescence rate in the experiments may have been sufficiently slow to allow the development of stress shadows between yielding and failure in some experiments, leading to delocalization; while in the other experiments, these rates may have been high enough to produce continuous localization until macroscopic failure.

4.2. Greater localization of volumetric strain than deviatoric strain

Laboratory observations show that dilation is a general phenomenon in low porosity crystalline rocks during triaxial compression (e.g., *Bridgman*, 1949; *Brace et al.*, 1966; *Paterson & Wong,* 2005; *Jaeger et al.*, 2009). These observations indicate that the macroscopic dilation of low porosity rocks subjected to increasing differential stress arises from the opening and propagation of fractures aligned parallel to the maximum compression direction. The contribution of dilation to the microscopic failure process has been difficult to directly compare to the contribution of shear deformation. Polarity and moment tensor inversions of acoustic emissions can constrain the relative contribution of the seismic tensile and shear deformation events (e.g., *Stanchits et al.*, 2006; *Graham et al.*, 2010). Although some analyses have observed the localization of acoustic emissions toward macroscopic failure (e.g., *Lockner et al.*, 1991; *Lockner & Byerlee*, 1977), to our knowledge such analyses have yet to quantify the localization of the shear and tensile-dominated acoustic emissions.

Comparing the degree of localization of the volumetric and deviatoric strains in our data show that the volumetric strain localizes to a greater extent than the deviatoric strain (**Figure** 4, **Figure** 5, **Figure** 8). In a previous analysis on the same set of experiments, we examined how four strain components, the contraction, dilation, left-lateral and right-lateral shear strain, measured with the divergence and curl, interacted with each other (*McBeck, Ben-Zion et al.*, 2020). This work found that the dilative strains occupy larger volumes and the contractive strains occupy smaller volumes with loading (e.g., **Figure** 8a). In contrast, the left- and right-lateral shear strain do not tend to occupy increasingly large volumes. This result occurs because the rocks experience increasing volume fractions of dilation, rather than contraction throughout loading. The shear strain, in contrast, does not experience a similar evolution in which one of the components systematically increases in volume while the other decreases. In the present work, we examine the localization of the largest magnitudes of the strain populations. Instead of examining the localization properties of the dilation and contraction separately, we compare the localization of the complete volumetric component to the deviatoric component. While the previous work found that the dilative strains dominate an increasingly larger volume of the system with loading, producing smaller and smaller volumes that experience contraction (e.g., **Figure** 8a), the present work finds that the high magnitudes of the volumetric strain localize to a greater extent than the high magnitudes of the deviatoric strains (e.g., **Figure** 8b).

Thus, the localization of the high magnitudes of the volumetric strain may better indicate the onset of the precursory phase preceding large earthquakes than the deviatoric strain. This implication depends on the ability of triaxial compression experiments to produce processes that occur in the crust preceding earthquakes. Earthquakes generally occur on preexisting faults that have experienced some degree of healing. Thus, the process leading to large earthquakes may require the breakage of some cohesive fault material or rock preceding aseismic or seismic slip, similar to these triaxial compression experiments on rock cores. However, the localization processes leading to large earthquakes in the crust may differ from macroscopic failure in these experiments because the rock cores do not include a healed fault zone with a lower strength and stiffness than the surrounding host rock. Such a fault zone would likely influence strain localization to a degree that depends on the ratio of the fault strength and stiffness to the host rock. For example, relatively strong and stiff fault zones with mechanical properties similar to the host rock may not exert a significant influence on strain localization. Differences in the strain localization process between the laboratory and the crust may also arise if the spatial scale influences this process. If the inferences from these experiments apply to crustal earthquakes, these results highlight the importance of monitoring changes of volumetric strain in crustal data, as well as the more prevalent monitoring of the deviatoric strain. Because the volumetric strain around large faults is associated with a shorter wavelength than the deviatoric strain (*Lyakhovsky & Ben-Zion*, 2020), monitoring the evolution of volumetric strain may require near-fault data.

The degree to which each strain component locally weakens the rock may control the observed difference in localization. Tensile deformation may produce a larger decrease in the local strength than shear deformation, even if the shear deformation initially hosts a tensile component, i.e., the deformation is mixed mode. Evidence for the greater influence of tensile deformation on macroscopic strength than shear deformation includes laboratory observations that show that jointed rocks tend to fail at lower stresses than fractured rocks (e.g., *Barton*, 2013). In addition, the damage parameter, *D*, in continuum damage mechanics models depends on the density and geometry of cracks and pores (e.g., *Kachanov*, 1986), suggesting that the mechanical strength of a rock is closely tied to the fracture density, and thus effective rock density and elastic moduli.

On a microscopic scale, if a fracture opens, slides and then closes, the resulting local decrease in strength would be less than if a fracture remains open. A fracture that opens and then slides may be more likely to close than a fracture that opens without additional sliding. Assuming a fracture is optimally oriented for sliding following the Coulomb criterion, inclined to σ_1, the orientation of the principal stresses acts to close the fracture once it stops sliding. In contrast, if the fracture is more optimally oriented for tensile failure, with σ_1 parallel to the fracture, then this stress state is less conducive to fracture closing than when the fracture is inclined to σ_1. Thus, tensile deformation may weaken rocks to a greater extent than shear deformation because open fractures may remain open while sliding fractures may close, producing a greater decrease in local density at open fractures.

Geologic evidence for this mechanical argument includes fractures that host minerals that form in the presence of water and appear to have opened parallel to σ_1, indicating that these fractures opened and remained open as minerals crystallized inside of them, with potentially repeated episodes of opening and closing (e.g., *Fisher & Brantley, 1992; Robert et al.,* 1995*; Parnell et al*., 2000; *Hilgers & Urai*, 2002). Additional evidence for this idea arises from analytical formulations of the stress intensity factor surrounding a sliding fracture with wing-cracks propagating at its tips, and the implications for the stability of this type of fracture growth. Propagation tends to decrease the stress intensity factor at the tip of these wing-cracks because they propagate further from the tensile stress concentration at the tip of the sliding crack, and the normal traction acting on the wing-crack inhibits additional propagation (*Paterson & Wong*, 2005 pg. 119-120). Both of these effects increase with wing-crack length. Thus, unless a wing-crack begins to interact with a neighboring crack, it will stop propagating under a given load. In contrast, the mode-I stress intensity factor increases with fracture length. These arguments suggest that shear deformation may be more likely to produce quasi-static crack growth than tensile deformation.

If a fracture dominated by tension tends to remain open more than a fracture dominated by shear, then dilative deformation will likely locally weaken the rock to a greater extent than shear deformation. This local weakening provides a positive feedback loop that localizes deformation: tensile deformation opens fractures, the local surrounding rock volume loses strength, and these conditions promote subsequent fracture nucleation, propagation, and opening. Evidence for this idea includes the well-observed coupling between 1) strain-weakening and localization, and 2) strain-hardening and delocalization (e.g., *Rudnicki & Rice*, 1975). For example, when deformation band development reduces the local porosity, it can increase the strength and stiffness of the host rock. This strengthening promotes subsequent deformation adjacent to the existing deformation band, rather than within it, because the higher porosity rock is weaker than the deformation band (e.g., *Mair et al*., 2000). Thus, deformation that increases the local porosity (i.e., tensile dominated deformation) is likely to have a localizing influence, while deformation that decreases the porosity is likely to delocalize subsequent deformation.

Shear zones provide additional evidence of strain-hardening coupled to distributed deformation, and strain-weakening coupled to localized deformation. Similar to deformation bands, strain-hardening produces widening shear zones, whereas strain-weakening produces localizing shear zones (e.g., *Vitale & Mazzoli*, 2008). More generally, strain weakening seems to be required for localization (e.g., *Tullis et al*., 1982; *Hobbs et al*., 1990). For example, bifurcation analysis uses the phenomena of localization to predict the conditions leading to macroscopic failure (e.g., *Rudnicki & Rice*, 1975). This theory aims to describe the conditions under which a uniform deformation field bifurcates into two solutions, or fields, that correspond to the localized deformation within a shear band, and the uniform deformation outside the band. The constitutive equations that describe this theory depend on the internal friction coefficient, a dilatancy factor, and a hardening modulus. The hardening modulus is positive when the system is strain-hardening and negative when the system is strain-weakening. Bifurcation analysis aims to find the critical hardening modulus at the onset of shear localization. Thus, the weakening or hardening behavior of a material is explicitly linked to the localization of deformation in this analysis. Therefore, deformation (dilation) that weakens the rock to a greater extent than another type of deformation (shear) is likely to produce greater localization than the other component. Thus, our experiments support this inference from bifurcation theory.

5. Conclusions

We quantified the localization of the volumetric and deviatoric strain components throughout twelve triaxial compression experiments imaged with X-ray tomography. We observe that 83% of the measured strain component evolutions show localization from the onset of loading to failure. Thus, although the vast majority of the experiments sustain strain localization, not all of them show this signal. Thus, assuming that our laboratory observations are relevant at the crustal scale, the localization of seismicity surrounding large tectonic faults may not occur preceding all large earthquakes. For example, creeping faults may generally localize strain, but also produce episodes of delocalization before moderate and large events, such as the observed delocalization of seismicity preceding the M6 Parkfield 2004 earthquake (*Ben-Zion & Zaliapin*, 2020).

Although most experiments show localization from the onset of loading until failure, the majority of the strain components do not achieve their maximum localization immediately preceding failure. Instead, only 46% of the measurements achieve their maximum localization in this final stage preceding failure. On average, the maximum localization occurs at 90% of the failure stress. These observations agree with the localizing seismicity observed before large earthquakes in southern and Baja California (*Ben-Zion & Zaliapin*, 2020): for some of the earthquakes with localizing seismicity, the system achieves its maximum localization in the 1-2 years preceding the main event, and not immediately before the event.

Tracking the maximum localization achieved by the volumetric and deviatoric strain components, and how this localization evolves throughout loading, indicates that the volumetric strain localizes to a greater extent than the deviatoric strain, and achieves greater magnitudes of localization throughout loading. The volumetric strains may localize more than the deviatoric strains because dilation may tend to weaken the local rock volume to a greater extent than the shear strain. These observations support using localization of the volumetric strain, rather than the deviatoric strain, to identify the onset of the precursory phase preceding large earthquakes.

Acknowledgements

We acknowledge the European Synchrotron Radiation Facility for provision of synchrotron radiation facilities (LTP ES-295). We would like to thank Benoît Cordonnier, Elodie Boller, Paul Tafforeau, and Alexander Rack for assistance in using beamline ID19 andSanchez Technologies for building the deformation apparatus. The Norwegian Research Council (grant 300435 to JAM) and U.S. Department of Energy (award DE-SC0016520 to YBZ) funded this work. The experimental data (time series of X-ray tomograms) are available on Norstore (project NS9073K). *Renard et al*. (2017), *Renard et al*. (2018), *Renard, McBeck, Cordonnier et al*. (2019), *Renard, McBeck, Kandula et al*. (2019), *McBeck et al*. (2019), *McBeck et al*. (2018), and *McBeck et al*. (2020) describe the sandstone, basalt, monzonite, granite, shale, and limestone experiments, and how to access these data. We thank Editor L. Chen and three anonymous reviewers for useful suggestions that helped us to improve the manuscript.

References

Autin, J., Bellahsen, N., Leroy, S., Husson, L., Beslier, M. O., & d'Acremont, E. (2013). The role of structural inheritance in oblique rifting: Insights from analogue models and application to the Gulf of Aden. Tectonophysics, 607, 51-64.

Barton, N. (2013). Shear strength criteria for rock, rock joints, rockfill and rock masses: Problems and some solutions. Journal of Rock Mechanics and Geotechnical Engineering, 5(4), 249-261.

Baud, P., Hall, S., Heap, M. J., Ji, Y., & Wong, T. F. (2021). The Brittle-Ductile Transition in Porous Limestone: Failure Mode, Constitutive Modeling of Inelastic Deformation and Strain Localization. Journal of Geophysical Research: Solid Earth, 126(5), e2020JB021602.

Ben-Zion, Y. (2008). Collective behavior of earthquakes and faults: Continuum-discrete transitions, progressive evolutionary changes, and different dynamic regimes. Reviews of Geophysics, 46(4).

Ben-Zion, Y., & Sammis, C. G. (2003). Characterization of fault zones. Pure and applied geophysics, 160(3), 677-715.

Ben-Zion, Y., & Zaliapin, I. (2019). Spatial variations of rock damage production by earthquakes in southern California. Earth and Planetary Science Letters, 512, 184-193

Ben-Zion, Y., & Zaliapin, I. (2020). Localization and coalescence of seismicity before large earthquakes. Geophysical Journal International, 223(1), 561-583.

Bennett, R. A., Wernicke, B. P., Niemi, N. A., Friedrich, A. M., and Davis, J. L. (2003), Contemporary strain rates in the northern Basin and Range province from GPS data, Tectonics, 22, 1008, doi:10.1029/2001TC001355, 2.

Bos, A. G., Spakman, W., and Nyst, M. C. J. (2003), Surface deformation and tectonic setting of Taiwan inferred from a GPS velocity field, J. Geophys. Res., 108, 2458, doi:10.1029/2002JB002336, B10.

Brace, W., Paulding Jr, B. W., & Scholz, C. H. (1966). Dilatancy in the fracture of crystalline rocks. Journal of geophysical research, 71(16), 3939-3953.

Bridgman, P. W. (1949). Volume changes in the plastic stages of simple compression. Journal of Applied Physics, 20(12), 1241-1251.

Charalampidou, E. M., Hall, S. A., Stanchits, S., Lewis, H., & Viggiani, G. (2011). Characterization of shear and compaction bands in a porous sandstone deformed under triaxial compression. Tectonophysics, 503(1-2), 8-17.

Cooke, M. L., & Madden, E. H. (2014). Is the Earth lazy? A review of work minimization in fault evolution. Journal of Structural Geology, 66, 334-346.

Fisher, D. M., & Brantley, S. L. (1992). Models of quartz overgrowth and vein formation: deformation and episodic fluid flow in an ancient subduction zone. Journal of Geophysical Research: Solid Earth, 97(B13), 20043-20061.

Graham, C. C., Stanchits, S., Main, I. G., & Dresen, G. (2010). Comparison of polarity and moment tensor inversion methods for source analysis of acoustic emission data. International journal of rock mechanics and mining sciences (Oxford, England: 1997), 47(1), 161.

Gini, C. (1921). Measurement of inequality of incomes. The economic journal, 31(121), 124-126.

Hatem, A. E., Cooke, M. L., & Toeneboehn, K. (2017). Strain localization and evolving kinematic efficiency of initiating strike-slip faults within wet kaolin experiments. Journal of Structural Geology, 101, 96-108.

Heap, M. J., Baud, P., McBeck, J. A., Renard, F., Carbillet, L., & Hall, S. A. (2020). Imaging strain localisation in porous andesite using digital volume correlation. Journal of Volcanology and Geothermal Research, 404, 107038.

Hilgers, C., & Urai, J. L. (2002). Microstructural observations on natural syntectonic fibrous veins: implications for the growth process. Tectonophysics, 352(3-4), 257-274.

Hobbs, B. E., Mühlhaus, H. B., & Ord, A. (1990). Instability, softening and localization of deformation. Geological Society, London, Special Publications, 54(1), 143-165.

Jaeger, J. C., Cook, N. G., & Zimmerman, R. (2009). Fundamentals of rock mechanics. John Wiley & Sons.

Jamtveit, B., Ben-Zion, Y., Renard, F., & Austrheim, H. (2018). Earthquake-induced transformation of the lower crust. Nature, 556(7702), 487-491.

Ji, Y., Hall, S. A., Baud, P., & Wong, T. F. (2015). Characterization of pore structure and strain localization in Majella limestone by X-ray computed tomography and digital image correlation. Geophysical Journal International, 200(2), 701-719.

Kachanov, L. (1986). Introduction to continuum damage mechanics (Vol. 10). Martinus Nijoff Publishers, Dordrecht, The Netherlands.

Lockner, D., & Byerlee, J. D. (1977). Hydrofracture in Weber sandstone at high confining pressure and differential stress. Journal of Geophysical research, 82(14), 2018-2026.

Lockner, D., Byerlee, J. D., Kuksenko, V., Ponomarev, A., & Sidorin, A. (1991). Quasi-static fault growth and shear fracture energy in granite. Nature, 350(6313), 39-42.

Lyakhovsky, V., & Ben-Zion, Y. (2009). Evolving geometrical and material properties of fault zones in a damage rheology model. Geochemistry, Geophysics, Geosystems, 10(11).

Lyakhovsky, V., & Ben-Zion, Y. (2020). Isotropic seismic radiation from rock damage and dilatancy. Geophysical Journal International, 222(1), 449-460.

Lyakhovsky, V., Ben-Zion, Y., & Agnon, A. (2001). Earthquake cycle, fault zones, and seismicity patterns in a rheologically layered lithosphere. Journal of Geophysical Research: Solid Earth, 106(B3), 4103-4120.

Mair, K., Main, I., & Elphick, S. (2000). Sequential growth of deformation bands in the laboratory. Journal of Structural Geology, 22(1), 25-42.

Mao, L., Liu, H., Lei, Y., Wu, J., Ju, Y., & Chiang, F. P. (2021). Evaluation of Global and Local Digital Volume Correlation for Measuring 3D Deformation in Rocks. Rock Mechanics and Rock Engineering, 1-16.

Mazzotti, S., & Gueydan, F. (2018). Control of tectonic inheritance on continental intraplate strain rate and seismicity. Tectonophysics, 746, 602-610.

McBeck, J. A., Aiken, J. M., Mathiesen, J., Ben-Zion, Y., & Renard, F. (2020). Deformation precursors to catastrophic failure in rocks. Geophysical Research Letters, 47, e2020GL090255.

McBeck, J., Aiken, J. M., Ben-Zion, Y., & Renard, F. (2020). Predicting the proximity to macroscopic failure using local strain populations from dynamic in situ X-ray tomography triaxial compression experiments on rocks. Earth and Planetary Science Letters, 543, 116344.

McBeck, J., Ben-Zion, Y., & Renard, F. (2020). The mixology of precursory strain partitioning approaching brittle failure in rocks. Geophysical Journal International, 221(3), 1856-1872.

McBeck, J., Cooke, M., & Madden, E. (2017). Work optimization predicts the evolution of extensional step overs within anisotropic host rock: Implications for the San Pablo Bay, CA. Tectonics, 36(11), 2630-2646.

McBeck, J., Kandula, N., Aiken, J. M., Cordonnier, B., & Renard, F. (2019). Isolating the factors that govern fracture development in rocks throughout dynamic in situ X-ray tomography experiments. Geophysical Research Letters, 46(20), 11127-11135.

McBeck, J., Kobchenko, M., Hall, S. A., Tudisco, E., Cordonnier, B., Meakin, P., & Renard, F. (2018). Investigating the onset of strain localization within anisotropic shale using digital volume correlation of time-resolved X-ray microtomography images. Journal of Geophysical Research: Solid Earth, 123(9), 7509-7528.

McBeck, J. A., Zhu, W., & Renard, F. (2021). The competition between fracture nucleation, propagation, and coalescence in dry and water-saturated crystalline rock. Solid Earth, 12(2), 375-387.

Parnell, J., Honghan, C., Middleton, D., Haggan, T., & Carey, P. (2000). Significance of fibrous mineral veins in hydrocarbon migration: fluid inclusion studies. Journal of Geochemical Exploration, 69, 623-627.

Paterson, M. S., & Wong, T. F. (2005). Experimental rock deformation-the brittle field. Springer Science & Business Media.

Peng, S. & Johnson, A.M. (1972). Crack growth and faulting in cylindrical specimens of Chelmsford granite. International Journal of Rock Mechanics and Mining Sciences & Geomechanics Abstracts, 9(1), 37-86.

Powers, P. M., & Jordan, T. H. (2010). Distribution of seismicity across strike-slip faults in California. Journal of Geophysical Research: Solid Earth, 115(B5).

Renard, F., Cordonnier, B., Dysthe, D. K., Boller, E., Tafforeau, P., & Rack, A. (2016). A deformation rig for synchrotron microtomography studies of geomaterials under conditions down to 10 km depth in the Earth. Journal of Synchrotron Radiation, 23(4), 1030-1034.

Renard, F., Cordonnier, B., Kobchenko, M., Kandula, N., Weiss, J., & Zhu, W. (2017). Microscale characterization of rupture nucleation unravels precursors to faulting in rocks. *Earth and Planetary Science Letters*, *476*, 69-78.

Renard, F., McBeck, J., Cordonnier, B., Zheng, X., Kandula, N., Sanchez, J. R., Kobchenko, M., Noiriel, C., Zhu, W., Meakin, P., Fusseis, F., & Dysthe, D. K. (2019). Dynamic in situ three-dimensional imaging and digital volume correlation analysis to quantify strain localization and fracture coalescence in sandstone. Pure and Applied Geophysics, 176(3), 1083-1115.

Renard, F., McBeck, J., Kandula, N., Cordonnier, B., Meakin, P., & Ben-Zion, Y. (2019). Volumetric and shear processes in crystalline rock approaching faulting. Proceedings of the National Academy of Sciences, 116(33), 16234-16239.

Renard, F., Weiss, J., Mathiesen, J., Ben-Zion, Y., Kandula, N., & Cordonnier, B. (2018). Critical evolution of damage toward system-size failure in crystalline rock. *Journal of Geophysical Research: Solid Earth*, *123*(2), 1969-1986.

Robert, F., Boullier, A. M., & Firdaous, K. (1995). Gold-quartz veins in metamorphic terranes and their bearing on the role of fluids in faulting. Journal of Geophysical Research: Solid Earth, 100(B7), 12861-12879.

Rudnicki, J. W., & Rice, J. R. (1975). Conditions for the localization of deformation in pressure-sensitive dilatant materials. Journal of the Mechanics and Physics of Solids, 23(6), 371-394.

Shahin, G., Papazoglou, A., Marinelli, F., & Buscarnera, G. (2019). Simulation of localized compaction in Tuffeau de Maastricht based on evidence from X-ray tomography. International Journal of Rock Mechanics and Mining Sciences, 121, 104039.

Stamati, O., Roubin, E., Andò, E., & Malecot, Y. (2019). Tensile failure of micro-concrete: from mechanical tests to FE meso-model with the help of X-ray tomography. Meccanica, 54(4), 707-722.

Stanchits, S., Vinciguerra, S., & Dresen, G. (2006). Ultrasonic velocities, acoustic emission characteristics and crack damage of basalt and granite. Pure and Applied Geophysics, 163(5), 975-994.

Tapponnier, P., & Brace, W.F. (1976). Development of stress-induced microcracks in Westerly granite. International Journal of Rock Mechanics and Mining Sciences & Geomechanics Abstracts, 13(4), 103-112. Pergamon.

Tarayoun, A., Mazzotti, S., & Gueydan, F. (2019). Quantitative impact of structural inheritance on present-day deformation and seismicity concentration in intraplate deformation zones. Earth and Planetary Science Letters, 518, 160-171.

Tchalenko, J. S. (1970). Similarities between shear zones of different magnitudes. Geological Society of America Bulletin, 81(6), 1625-1640.

Tudisco, E., Andò, E., Cailletaud, R., & Hall, S. A. (2017). TomoWarp2: A local digital volume correlation code. SoftwareX, 6, 267-270.

Tullis, J., Snoke, A. W., & Todd, V. R. (1982). Significance and petrogenesis of mylonitic rocks. Geology, 10(5), 227-230

Vitale, S., & Mazzoli, S. (2008). Heterogeneous shear zone evolution: the role of shear strain hardening/softening. Journal of Structural Geology, 30(11), 1383-1395.

Zeng, Y., Petersen, M. D., & Shen, Z. K. (2018). Earthquake potential in California-Nevada implied by correlation of strain rate and seismicity. Geophysical Research Letters, 45(4), 1778-1785.